

LED: LLM Enhanced Open-Vocabulary Object Detection without Human Curated Data Generation

Yang Zhou Shiyu Zhao Yuxiao Chen Zhenting Wang Can Jin Dimitris N. Metaxas

Rutgers University

{eta.yang, sz553, yc984, zhenting.wang, can.jin, dnm}@rutgers.edu

Abstract

Large foundation models trained on large-scale vision–language data can boost Open-Vocabulary Object Detection (OVD) via synthetic training data, yet the hand-crafted pipelines often introduce bias and overfit to specific prompts. We sidestep this issue by *directly fusing* hidden states from Large Language Models (LLMs) into detectors—an avenue surprisingly under-explored. This paper presents a systematic method to enhance visual grounding by utilizing decoder layers of the LLM of a MLLM. We introduce a zero-initialized cross-attention adapter to enable efficient **knowledge-fusion** from LLMs to object detectors, an new approach called **LED** (LLM Enhanced Open-Vocabulary Object Detection). We find that intermediate LLM layers already encode rich spatial semantics; adapting only the early layers yields most of the gain. With Swin-T as the vision encoder, Qwen2-0.5B +LED lifts GroundingDINO by **3.82 %** on OmniLabel at just **8.7 %** extra GFLOPs, and a larger vision backbone pushes the improvement to **6.22 %**. Extensive ablations on adapter variants, LLM scales and fusion depths further corroborate our design.

1 Introduction

Open Vocabulary object Detection (OVD) localizes objects described by free-form text, significantly increasing the size of the label space and enabling broader applications, compared to the traditional closed-set object detection with a fixed label space. Significant prior efforts [16, 26, 36, 45, 46] focus on exploring large foundation models trained on image and/or text data to generate high-quality data for OVD, greatly boosting performance on challenge benchmarks [10, 30, 33]. Their success demonstrates that large foundation models implicitly capture rich semantic knowledge and reasoning capabilities through pretraining, which are beneficial for accurately localizing objects under complex, free-form textual queries.

However, existing methods rely on hand-crafted rules to query large foundation models for synthetic data. For example, VL-PLM [45] and OWLv2 [26] design a delicate procedure with heuristics to use pretrained vision and language models (VLMs) to generate pseudo labels for unseen categories that are not included in the human provided data. DesCo [16] and GenEnhancedNegs [47] assume that detailed or negative descriptions are important training signals for OVD, and thus leverage large language models (LLMs) to create those descriptions. Those methods are well designed for certain aspects (e.g. unseen categories and descriptions) to improve OVD models, **which are biased and cannot fully leverage knowledge gained during the pretraining of large foundation models**.

We argue that the *latent representations* of large multimodal language models already encode rich visual–linguistic concepts that need not be materialised into explicit labels. Building on this observation, we introduce LED, an Latent Enhanced Open-Vocabulary Object Detection that realises a **novel knowledge-fusion paradigm**: instead of learning a detector *from scratch* or augmenting training with generated data, we *directly fuse* intermediate hidden states from a frozen MLLM into popular mainstream detector via a lightweight adapter. Specifically, as shown in Figure 1(a), existing ap-

proaches primarily distill LLM knowledge into the object detector via explicit data generation—such as synthesizing negative examples to mitigate hallucinations [29, 37, 38, 42, 47], or creating detailed annotations of spatial and logical relationships [16]. However, these explicit generation methods inherently constrain model robustness and generalizability. In contrast, as illustrated in Figure 1(b), our method **directly fuses the high-dimensional semantic knowledge** encapsulated within LLM hidden states into the detector, thereby preserving richer pretrained knowledge without explicit data augmentation.

We apply LED to popular open-source object detectors. GroundingDino [21]. Our method significantly improves performance on prevailing benchmarks, including RefCOCO [40] and OmniLabel benchmark [30]. Besides, we find that hidden states from the first several layers of a MLLM are rich enough to improve the OVD models. Probably, **MLLMs focuses more on vision tokens in early layers and then on text tokens in later layers**, as illustrated in Section 3. Thus, vision tokens of deeper layers are not quite updated and embody similar knowledge as earlier ones.

Our contributions are summarized as:

- (1) We introduce a lightweight adapter that directly **fuses** frozen MLLM hidden representations into any object detector, establishing a unified knowledge-injection pipeline and eliminating the need for expensive data synthesis.
- (2) We systematically explore various fusion designs—layer selection, injection modality, adapter structure, etc.—and identify the most effective pipeline, offering clear guidelines for future work.
- (3) We conduct extensive experiments, demonstrating that our approach not only improves OVD models across various benchmarks, but also achieves benefits comparable or even better to those obtained through data generation.

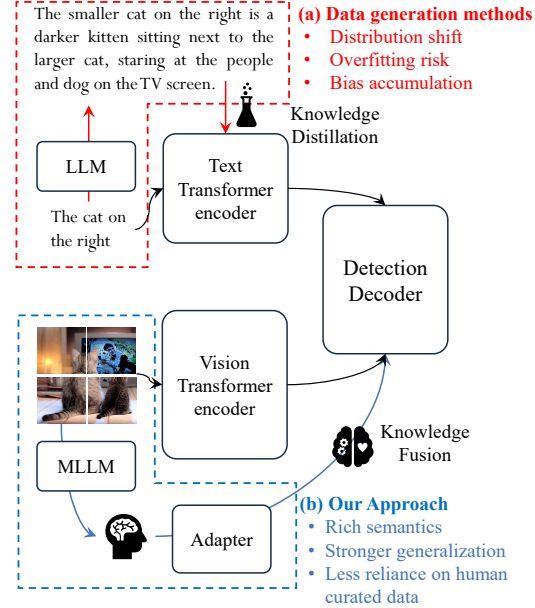


Figure 1: Overview of open vocabulary object detection approaches. (a) Data generation methods prone to distribution shift and overfitting; (b) Our proposed adapter-based framework directly leverages knowledge from the MLLM to the detection decoder.

2 Relate Work

Multi-Modal Large Language Models: Recent MLLMs have driven visual–language integration through modality alignment. CLIP pioneered contrastive learning on large-scale image–text pairs [27], and BLIP enhanced alignment with curated data [14, 15]. LLaVA applies GPT-4–generated multimodal instruction tuning to boost reasoning [20]. InternVL’s progressive alignment scales vision–language models to SOTA in foundation models [4–6, 9, 32]. LLaMA Adapter uses a zero-initialized attention mechanism with just 1.2 M parameters for prompt-based tuning, matching full fine-tuning [44]. LED instead fuses high-level MLLM embeddings directly into downstream detectors.

Open-Set Object Detection: While MLLMs excel at integrating textual and visual modalities, open-world detection remains an unsolved challenge that calls for more flexible category representations. DINO advances closed-set detection through contrastive de-noising in DETR frameworks [1, 43], its reliance on fixed category definitions limits open-world applicability. This motivates open-set detection methods that leverage language generalization: OV-DETR employs CLIP embeddings as cross-modal queries for category-agnostic box decoding [41], and GLIP reformulates detection as visual grounding with phrase-region alignment [8, 17]. GroundingDINO subsequently refines these grounding mechanisms, establishing new benchmarks in zero-shot detection [21].

Vision-Language Grounding: With open-set capabilities taking shape, further progress demands robust vision-language grounding that handles diverse and unconstrained data distributions. Recent advances in leveraging vision-language models (VLMs) for open-vocabulary and open-ended object detection predominantly rely on large-scale synthetic or generated datasets. Techniques such as prompt-driven visual-text adaptation [23, 35] and generative augmentation of negative samples [47] have significantly improved model performance by enriching training data with diversified visual and textual examples. Similarly, generative region-language pretraining frameworks [18] and unified object-centric grounding methods [28] also heavily rely on generated or automatically curated datasets, demonstrating their efficiency and scalability.

However, synthetic data often misaligns with real-world distributions, introducing biases that degrade performance under natural variations and unseen scenarios. Moreover, overreliance on generated samples can lead to overfitting to specific dataset artifacts, limiting adaptability in truly open-world settings. While approaches like GLIP [17] and DetCLIP [35] improve grounding via enriched annotations, their dependence on synthetic constructs remains a core limitation.

3 Methodology

Our framework establishes an efficient pipeline for transferring multimodal knowledge from LLMs to OVD models via intermediate feature adaptation. As shown in Figure 2, we analyze token attention changes across different layers of the LLM decoder for Qwen2-0.5B. In the early layers of the LLMs decoder (e.g., layers 0 to 4), the median attention score decreases significantly and fluctuates slightly in the subsequent 20 layers. This indicates that the **MLLMs already exhibit strong attention or encoding capabilities for input image tokens in the early layers**, while the later layers may focus more on fine-tuning task- or semantics-related text tokens Section A.1 (in the supplement).

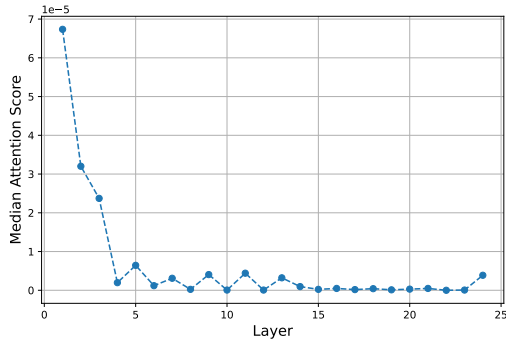


Figure 2: Median distribution of attention scores across different layers in Qwen2-0.5B decoder.

To validate this concept, we design an architecture illustrated in Figure 3. The architecture comprises four key components: (1) an efficient cross-modal alignment strategy in Section 3.1; (2) an MLLM for semantic adaptation prompts generation in Section 3.2; (3) a universal end-to-end detector in Section 3.3; (4) a zero-initialized cross-attention adapter for feature fusion Section 3.4.

3.1 Cross-modal Alignment

LED aims to provide a comprehensive solution by leveraging the extensive knowledge of LLMs to enhance semantic image understanding. In general, MLLMs for text and images require a vision encoder to generate visual tokens for LLMs. Thus, cross-modal alignment is crucial for ensuring that LLMs can interpret the visual tokens generated by the vision encoder and assign semantic meaning to them. To facilitate effective knowledge transfer while maintaining computational efficiency, we establish a shared vision encoder between the MLLM and the detector through a three-stage alignment process:

Stage 1 - Pretraining: We employ a vision encoder and LLM to pretrain the MLP projection layer to align feature spaces.

Stage 2 - Finetuning: We fine-tune the model on a specific task dataset to align the vision encoder and LLM at a fine-grained level and improve instruction-following capabilities.

Stage 3 - Adapter Training: With the MLLM and detector frozen, we train the grounding decoder adapter (Block 3) and the MLP layer and LLM in the MLLM to integrate semantic cues from its intermediate features, thereby enabling the LLM to better focus on grounding tasks when processing visual tokens.

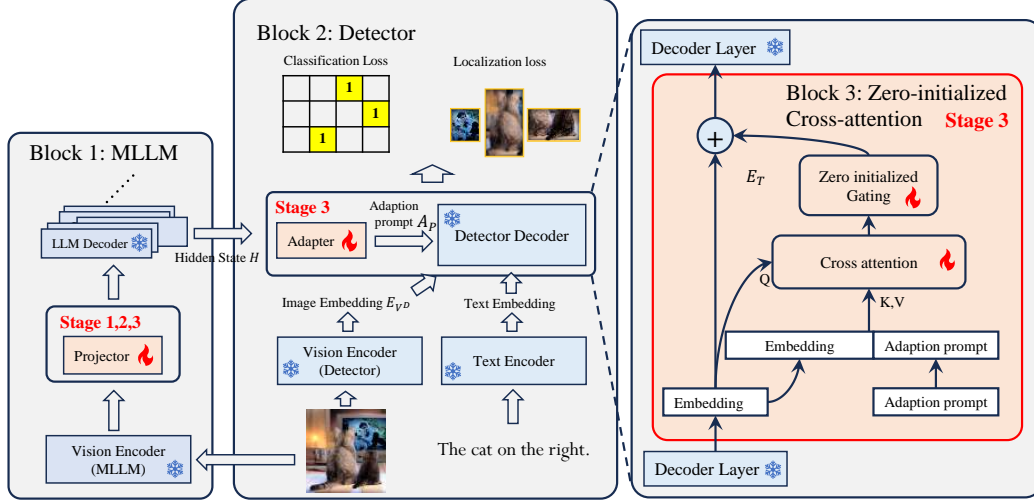


Figure 3: The architecture of LED. We present the overall architecture, MLLM, detector, zero-initialized cross-attention in Block 1, 2, 3, respectively. In stage 1 and 2, a trained projector is used to align the frozen Vision Encoder with the LLM. In stage 3, a zero-initialized adapter is trained to guide the detector with adaptation prompts, while the projector still participate training to adapt to downstream tasks.

3.2 Semantic Prompt Generation

As illustrated in Figure 3 Block 1, we employ an MLLM that processes the same input images shared with the detector. The MLLM integrates visual features with system prompts and provides the resulting embeddings as input to the LLM.

We extract intermediate representations from the ℓ_{LM} -th decoder layer of an n -layer language model, referred to as the hidden state embedding \mathbf{H} . After obtaining the \mathbf{H} , the vision embedding \mathbf{E}_V^L and text embeddings \mathbf{E}_T are derived by truncating the embeddings based on the positions of the image and text tokens:

$$\begin{aligned} \mathbf{H}_{\ell_{LM}} &= \text{Decoder}_{\ell_{LM}}(\mathbf{H}_{\ell_{LM}-1}), \ell_{LM} \in \{1, \dots, n\} \\ \mathbf{E}_V^L, \mathbf{E}_T &= \text{Truncate}(\mathbf{H}_{\ell_{LM}}) \end{aligned} \quad (1)$$

3.3 Grounding Detector

An End-to-End Transformer-based Detector architecture, as shown in Figure 3 Block 2. For every (Image, Text) pair, this Block employs a vision encoder and a text encoder to independently extract visual and textual features. These features are then passed into a cross-modality decoder, which interacts with both modalities to refine and update the features. The final output queries generated by the last layer of the decoder are used to predict bounding boxes for objects and extract their corresponding textual phrases [1, 21, 43].

3.4 Zero-initialized Cross-attention

An adapter design (Block 3 in Figure 3) effectively refines the vision embedding \mathbf{E}_V^L and text embedding \mathbf{E}_T from the LLM to generate adaptation prompts with detector features through zero-initialized cross-attention. We apply a convolutional layer to process the MLLM’s vision embeddings \mathbf{E}_V^L to get adaptation prompts \mathbf{A}_P .

$$\mathbf{A}_P = \text{Conv2D}(\mathbf{E}_V^L) \in \mathbb{R}^{B \times L \times d} \quad (2)$$

where B is batch size, L is the length of adaptation prompts, decomposed into the height h and width w of the Vision embedding \mathbf{E}_V^L when performing convolution processing.

A zero-initialized cross-modal attention mechanism is designed based on a small gating unit. It is worth noting that since the weights of the entire adapter are randomly initialized, directly providing the adaptation prompt to the detector decoder introduces disordered noise, which is detrimental to the training of the network. Given a decoder embedding $\mathbf{E}_D^{\ell_D} \in \mathbb{R}^{B \times T \times d}$ from ℓ_D th decoder layer and adaptation prompts $\mathbf{A}_P \in \mathbb{R}^{B \times L \times d}$, our zero-initialized cross-modal attention mechanism operates as follows:

$$\begin{aligned}\mathbf{Q} &= \mathbf{E}_D \mathbf{W}_Q \in \mathbb{R}^{B \times T \times h \times d_h} \\ \mathbf{K} &= \mathcal{C}(\mathbf{A}_P \cdot \mathbf{W}_K, \mathbf{E}_D \mathbf{W}_K) \in \mathbb{R}^{B \times (L+T) \times h \times d_h} \\ \mathbf{V} &= \mathcal{C}(\mathbf{A}_P \cdot \mathbf{W}_V, \mathbf{E}_D \mathbf{W}_V) \in \mathbb{R}^{B \times (L+T) \times h \times d_h}\end{aligned}\quad (3)$$

where $\mathcal{C}(\cdot)$ denotes concatenation along the sequence dimension, h is the number of attention heads, and $d_h = d/h$ represents the dimension per head. $\mathbf{W}_Q, \mathbf{W}_K, \mathbf{W}_V$ are the linear projection matrices used in the attention mechanism to map to Q, K, V .

$$\begin{aligned}\mathbf{S} &= \frac{\tilde{\mathbf{Q}}\tilde{\mathbf{K}}^\top}{\sqrt{d_h}} + \mathbf{M} \in \mathbb{R}^{B \times h \times T \times (L+T)} \\ \tilde{\mathbf{S}} &= \mathcal{C}(\tanh(\mathbf{g}) \odot \text{softmax}(\mathbf{S}_{:,0:L}), \text{softmax}(\mathbf{S}_{:,L+1:L+T})) \in \mathbb{R}^{B \times h \times T \times (L+T)}\end{aligned}\quad (4)$$

where $\tilde{\mathbf{Q}}, \tilde{\mathbf{K}}$ is defined as $\text{RoPE}(\mathbf{Q}, \mathbf{K}; \Theta)$ with angular parameter matrix Θ ; \mathbf{S} represents the raw attention score matrix, and $\tilde{\mathbf{S}}$ is attention weight matrix obtained by applying softmax; $\mathbf{g} \in \mathbb{R}^{1 \times h \times 1 \times 1}$ is a learnable gating vector initialized to $\mathbf{0}$, and an activation function $\tanh(\cdot)$ is adopted to regulate the scale of \mathbf{g} to into $-1 \sim 1$. If adaptation prompts are initialized randomly, they may introduce noise or interfere with word tokens during the initial stages of training, thereby compromising the stability and effectiveness of the fine-tuning process.

Finally a linear projection layer calculate the output as adaptation prompts and add on decoder embedding from ℓ_D th decoder layer as:

$$\mathbf{E}_D^{\ell_D} = \mathbf{E}_D^{\ell_D-1} + \text{Linear}(\tilde{\mathbf{S}}\mathbf{V}) \in \mathbb{R}^{B \times T \times d} \quad (5)$$

4 Experiments

In this section, we first detail the datasets and implementation specifics Section 4.1). Next, through evaluations on the OmniLabel benchmark[30], we analyze strategies for sharing vision decoder features (see Section 4.2.1), investigate the impact of different adapter architectures (see Section 4.2.3), and observe performance improvements across various scales of LLMs for visual detection and grounding tasks (see Section 4.2.3). Finally, we conduct ablations to precisely quantify the contributions of MLLM decoder hidden states at various layers to detection performance (see Section 4.4).

4.1 Dataset and Implementation Details

MLLMs alignment: The dataset used to train the projector follows the approach outlined in the ShareGPT-4V plan [3]. Our architecture adopts a multi-stage training paradigm, incorporating a carefully designed data composition. For *InternVL2-1B*, we employ a **two-phase strategy**:

Stage 1: We leverages LAION-CC-SBU (558K samples) [19] to establish cross-modal alignment through diverse visual-linguistic interactions.

Stage 2: We combine ShareGPT4V (102K) and SFT (665K) [3] for instruction tuning, augmented with domain-specific datasets Section D.1 (see Supplement) to enhance structured visual understanding.

Stage 3 - Adapter training: We employ Grounding DINO [21] pretrain on Object365, GoldG and Cap4M as a unified detection pre-training framework across three datasets: Object365 [31], COCO2017, and Flickr30k [39]. We implement our framework using InternVL2-1B (Qwen2-0.5B backbone) as the MLLM [4–6, 9, 32] and Open-GroundingDINO [21] as the detection codebase. ALL experiment configuration As shown in Section A.3 (see Supplement)

Table 1: Model params, compute cost, and inference latency; most overhead stems from the LLM’s two layers, with minimal adapter cost.

Framework	Params	GFLOPs	Latency
G-DINO	172M	412G	299.3 ms
LED	+58M	+36G	+52.3ms
-Adapter	+2.2M	+2.0G	+2.0ms
-Qwen2-0.5B 2_L	+56M	+34G	+50.5ms

Table 2: OmniLabel evaluation for the three-stage pipeline and shared vision decoder, relative to GroundingDINO.

OmniLabel	AP descr, categ	AP categ	AP descr
G-DINO	21.69%	33.25%	16.09%
Swin-T+	25.51%	33.01%	20.28%
Qwen2-0.5B	↑3.82%	↑0.25%	↑4.19%

4.2 Evaluation

We evaluated and analyzed adapters under different architectures based on the OmniLabel benchmark [30]. Additionally, we compared the performance results of the hidden state acquisition scheme in InternVL2 with GroundingDINO (abbreviated as G-DINO in tables).

4.2.1 Vision Decoder Share from Detector

The rich semantic understanding of the MLLM primarily originates from the LLM rather than the vision encoder. Thus, we adopt GroundingDINO’s vision encoder architecture and weights to provide visual inputs for both the detector and MLLM. We conduct MLLM training in two stages (see Figure 3): pretraining (stage 1) and finetuning (stage 2), freezing both the vision encoder and LLM during training. Section A.5 (supplementary) provides MME evaluations of alignment progress between stages.

Specifically, the shared Swin-Tiny vision encoder output undergoes a pixel shuffle operation (scaling factor 4), reducing spatial dimensions (h, w) by a factor of 4 while expanding the channels by a factor of 16. This transformed output is then truncated to match the MLP projection layer dimension (4096), aligning the feature spaces through pretrained MLP layers:

$$\hat{f}_v = \text{MLP}(\text{Truncate}(\text{Repeat}(\text{PixelShuffle}_4(\text{Vision Encoder}(I)))))) \quad (6)$$

where I denotes the input image and \hat{f}_v represents the visual features projected. $\text{PixelShuffle}_4(\cdot)$ denotes the pixel shuffle operation with a scaling factor of 4, $\text{Repeat}(\cdot)$ represents the repetition of channels, $\text{Truncate}(\cdot)$ ensures that the channel dimension matches the MLP’s input requirements.

Finally, when training the adapter (stage 3 in Figure 3), both the LLM and the MLP layers are trained simultaneously to adapt to downstream tasks. Image embeddings from Swin-Tiny (used in GroundingDINO) are fed into the LLM after alignment by a projector. The pretrained weights for Swin-Tiny, which are the same as those used in GroundingDINO and provided by Open-GroundingDINO [48], are utilized and frozen during every stage.

We measured the GFLOPs for each architecture and selected the 2_{nd} decoder layer, removing subsequent layers. As shown in Table 1, LED requires only 8.7% more FLOPs than GroundingDINO, with the majority of the computational cost attributed to the LLM’s decoder.

The OmniLabel benchmark [30] for our method is presented in Table 2 with an improvement of 3.82% over GroundingDINO. This gain stems from the adaptation prompts generated by the LLM.

4.2.2 Adapter Architecture Analysis

In MLLMs, how the vision encoder aligns with the LLM decisively affects image-token understanding. We adopt the InternVL ViT backbone (pre-trained) for InternVL2-1B/2B/8B and compare four adapter designs that extract *adaptation prompts* from decoder hidden states while coping with truncated text embeddings.

Arch. I — Double Cross-Modal Fusion. As shown in the Figure 7 (in the supplement), owing to the robust cross-modal feature fusion capabilities of MLLMs, the text embeddings \mathbf{E}_T extracted from the hidden state, encompass substantial information relevant to image understanding. Furthermore, these embeddings can guide the Detector by leveraging user-provided instructions. The LLM input is

Method	AP descr,categ	AP categ	AP descr
G-DINO	21.69%	33.25%	16.09%
Arch. I	22.57% $\uparrow 0.88\%$	33.80% $\uparrow 0.55\%$	16.95% $\uparrow 0.86\%$
Arch. II	24.52% $\uparrow 2.84\%$	31.05% $\downarrow 2.20\%$	20.26% $\uparrow 4.17\%$
Arch. III	24.63% $\uparrow 2.95\%$	32.07% $\downarrow 1.19\%$	19.99% $\uparrow 3.90\%$
Arch. IV	25.98% $\uparrow 4.29\%$	33.89% $\uparrow 0.63\%$	21.06% $\uparrow 4.97\%$

Table 3: OmniLabel evaluation for different adapter architectures. Architecture I: Full cross-attention fusion; II: Conv-based prompt projection; III: Early decoder injection; IV: Text-free adaptation.

formulated as a structured prompt that integrates task instructions and object captions, adhering to GroundingDINO’s annotation protocol:

'<user>: [Instruction: 'Detect objects in this image. If present, locate them with bounding boxes.']+ [Caption: 'The cat on the right']

We extract image/text embeddings $\mathbf{E}_T/\mathbf{E}_{V_D}$ from the decoder’s hidden states using positional segmentation. The cross-attention mechanism operates through two stages: (1) *Text-guided image fusion*: Image embeddings as queries attend to text embeddings (keys/values); (2) *Prompt-enhanced detection*: Detector queries attend to fused embeddings (keys/values)

Through two cross-attention mechanisms, we integrate the Adaptation prompt, which combines images and text, back into the Image embedding of the Detector through a zero-initialized gating:

$$\mathbf{A}_P = \text{Gating}(\text{CrossAtt}(\text{CrossAtt}(\mathbf{E}_V^L, \mathbf{E}_T), \mathbf{E}_{V_D})) \quad (7)$$

Arch. II — Late Prompt Projection. We drop the second cross-modal block. As shown in the Figure 8 (see Supplement), a $3 \times 3/2$ convolution maps the fused prompt to the detector space and injects it into the last decoder layer ($\ell_D=6$):

$$\mathbf{A}_P = \text{Conv2D}(\text{CrossAtt}(\mathbf{E}_V^L, \mathbf{E}_T)) \in \mathbb{R}^{B \times L \times d} \quad (8)$$

Then the adaptation prompts provide to the last cross-modal decoder layer $\ell_D = 6$, as the describe in Section 3.4.

Arch. III — Early Decoder Injection. Same as Arch. II but insert at the *first* decoder layer ($\ell_D=1$) for progressive refinement:

$$\mathbf{F}_i^{\ell_D} = \text{Decoder}_{\ell_D}(\mathbf{F}_i^{\ell_D-1}, \mathbf{P}), \ell_D \in \{1, \dots, 6\} \quad (9)$$

Arch. IV — Text-Free Adaptation. As shown in the Figure 4, Eliminating text embeddings \mathbf{E}_T , we directly project image embeddings \mathbf{E}_v using the same convolutional layer as Arch. II. This tests the hypothesis that visual embeddings alone carry sufficient multimodal signals.

As illustrated in the Table 3, Arch. II boosts descr-AP by +4.17% over Arch. I but sacrifices 2.20% categ-AP, implying that late fusion favours free-form phrases at the cost of categorical priors. Early injection (Arch. III) recovers part of the categ-AP while retaining most of the descr-AP. Surprisingly, text-free Arch. IV outperforms all others, suggesting (i) vision embeddings already encode rich cross-modal cues from pretraining, and (ii) naive text–vision fusion may introduce semantic noise without explicit contrastive alignment.

4.2.3 Different LLMs

We employ the InternVL-1B, 2B, and 8B models to extract the hidden state from the $\ell_{LM} = 2\text{nd}$ layer of the LLM decoder to generate the adaptation prompts. InternVL-1B, 2B, and 8B models are all based on InternViT-300M as the vision encoder, and they use Qwen2-0.5B, InternLM2-1.8B, and InternLM2.5-7B as the LLMs, respectively. Table 4 demonstrates the performance comparison between our method and Grounding DINO on the OmniLabel benchmark [30].

LED achieves significant improvements in open-set object detection, with 6.22% and 6.19% AP gains for LED Qwen2-0.5B and LED +InternLM2-1.8B, respectively. The attention mechanisms in LLM’s decoder layers effectively **fusing semantically knowledge** to visual features, enabling better grounding of complex object descriptions.

In particular, the description and positioning joint task shows remarkable 11.63% and 11.53% AP improvements, demonstrating MLLMs’ capacity for spatial relationship understanding. We hypothesize that this stems from the model’s strong logical reasoning capabilities, which enhance the understanding of spatial relationships in textual descriptions, such as "a person holding a phone." The visual-textual co-attention mechanisms likely help disambiguate spatial configurations that challenge pure visual encoders. This phenomenon is clearly observed in the analysis of Appendix C (see Supplement).

Notably, category detection shows minimal improvements (0.67% AP and 0.19% gain) across experiments because closed-set category recognition relies primarily on visual prototype matching rather than semantic understanding. Thus, the Swin-Tiny encoder’s features may already saturate performance on this conventional detection task, leaving limited room for text-guided enhancement.

We evaluated our model on RefCOCO+/g [40], and the results are shown in Table 5. Combining the evaluation results from OmniLabel, we found that: LED +Qwen2-0.5B shows comparable performance to LED +InternLM2.5-7B despite 14× more parameters. This suggests a pattern of diminishing returns in scaling LLMs for visual grounding, supporting the hypothesis from [7] that small models can suffice for certain vision–language mappings.

4.3 Comparison with synthetic-data baselines.

We integrate LED into the GLIP-T detector and evaluate on OmniLabel, juxtaposing it with two SOTA data-generation pipelines—NEG-Text [47] and DesCo [16]. Without synthesising any extra training data, LED attains the best overall score and the highest descr-AP.

OmniLabel	AP descr,catgeg	AP catgeg	AP descr	AP descr-pos
G-DINO	21.69%	33.25%	16.09%	24.61%
Qwen2-0.5B	27.90% $\uparrow 6.22\%$	33.93% $\uparrow 0.67\%$	23.70% $\uparrow 7.61\%$	36.24% $\uparrow 11.63\%$
InternLM2-1.8B	27.87% $\uparrow 6.19\%$	33.44% $\uparrow 0.19\%$	23.90% $\uparrow 7.81\%$	36.13% $\uparrow 11.53\%$
InternLM2.5-7B	26.33% $\uparrow 4.65\%$	32.03% $\downarrow 1.22\%$	22.36% $\uparrow 6.27\%$	34.34% $\uparrow 9.73\%$

Table 4: OmniLabel evaluation on GroundingDINO vs. adaptation prompts LED + Qwen2-0.5B, LED + InternLM2-1.8B and LED + InternLM2.5-7B.

	RefCOCO			RefCOCO+			RefCOCOg	
	eval	test A	test B	eval	test A	test B	eval	test
G-DINO	48.0%	54.8%	41.5%	48.5%	53.0%	44.1%	66.2%	66.4%
Qwen2-0.5B	51.3%	58.6%	43.4%	50.8%	56.0%	45.3%	70.2%	70.5%
	$\uparrow 3.3\%$	$\uparrow 3.8\%$	$\uparrow 1.9\%$	$\uparrow 2.3\%$	$\uparrow 3.0\%$	$\uparrow 1.2\%$	$\uparrow 4.0\%$	$\uparrow 4.1\%$
InternLM2.5-7B	52.4%	59.8%	45.1%	51.8%	57.2%	46.8%	71.2%	71.4%
	$\uparrow 4.4\%$	$\uparrow 5.0\%$	$\uparrow 3.6\%$	$\uparrow 3.3\%$	$\uparrow 4.2\%$	$\uparrow 2.7\%$	$\uparrow 5.0\%$	$\uparrow 5.0\%$

Table 5: Performance comparison on RefCOCO, RefCOCO+, and RefCOCOg datasets with improvements over GroundingDINO.

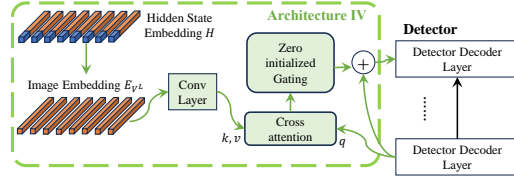


Figure 4: The adapter architecture IV of LED: We ultimately used image embedding part as the key and value for cross-attention. The query is derived from the embedding of the last detector decoder. The out of attention to the input of the next decoder through a zero-initialized gating.

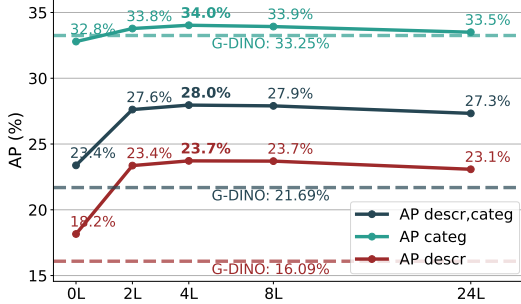


Figure 5: OmniLabel prompts evaluated across LLM decoder layers 0–24.

Table 6: OmniLabel performance (%) of LED based on InternVL2-1B (IVL2-1B) compare with SOTA GLIP-T-based data-generation pipelines.

Method	AP descr, categ	AP descr
GLIP-T [17]	19.3	16.4
NEG-TEXT [47]	22.2	18.8
DESCo [16]	23.8	21.0
LED IVL2-1B	24.8	24.7

As shown in the Table 6, LED achieves the highest overall score while requiring no synthetic labels, showcasing superior knowledge fusion over data-generation approaches. **Notably**, LED IVL2-1B particularly excels on the more challenging description samples, achieving a description AP of 24.7%, which is 3.7% higher than DesCo (21.0%), demonstrating its superior performance in complex semantic understanding and localization.

4.4 Deeper Decoder Layers Offer No Additional Benefit

To quantify the information contained at different decoder layers of the MLLM, we ablated adaptation prompts derived from each layer—including the pure ViT embeddings from the 0 “layer” (vision encoder only, without LLM)—and evaluated them on OmniLabel (see Figure 5). The ViT-only prompts yield minimal gains in the categorical AP, whereas prompts from early LLM decoder layers remain rich in semantic cues. In InternVL2-1B (24-layer Qwen2-0.5B), using only the first two decoder layers already yields significant improvements, with performance peaking at layer 4. **Notably**, deeper decoder layers do not guarantee better features. This aligns with our attention-map analysis in Section 3 and Figure 6 (see Supplementary), which shows that image processing completes in early layers, “condensing” most visual information into those representations.

4.5 Detector with LED vs. Direct-LLM Substitution

As shown in the Appendix B (see Supplementary), replacing the detector’s visual embeddings with raw hidden states extracted from a frozen MLLM not only fails to match the original detector’s performance but can even cause a dramatic collapse in detection accuracy, confirming that latent features alone are neither geometrically nor semantically aligned with the detector’s visual space. Effective transfer therefore requires an explicit knowledge-fusion mechanism that jointly conditions on both language and vision, and the specialized detector **remains indispensable** for reliable performance in vision–language tasks.

5 Conclusions

Our work introduces a systematic framework that leveraging early MLLM decoder layers to boost visual grounding efficiency. We (1) demonstrate that shallow Transformer hidden states preserve rich spatial–semantic correlations; (2) design a zero-initialized cross-attention adapter for seamless MLLM-to-detector knowledge transfer; and (3) develop two adaptation-prompt schemes that sharpen descriptive precision while maintaining category accuracy. Integrating Qwen2-0.5B with Swin-Tiny yields a 3.82% OmniLabel gain at just 8.7% extra GFLOPs, while swapping in InternVL ViT pushes the improvement to 6.22%, alongside notable RefCOCO+/g boosts. Extensive ablation studies across adapter variants, LLM scales, and decoder layers **confirm** our method’s robustness—especially for detailed and zero-shot queries. Our generalizable adapter design supports real-time vision–language applications and mitigates overfitting due to manual prompt bias, thereby advancing practical MLLM deployment.

References

- [1] Nicolas Carion, Francisco Massa, Gabriel Synnaeve, Nicolas Usunier, Alexander Kirillov, and Sergey Zagoruyko. End-to-end object detection with transformers. In *European conference on computer vision*, pages 213–229. Springer, 2020.
- [2] Liang Chen, Haozhe Zhao, Tianyu Liu, Shuai Bai, Junyang Lin, Chang Zhou, and Baobao Chang. An image is worth 1/2 tokens after layer 2: Plug-and-play inference acceleration for large vision-language models, 2024. URL <https://arxiv.org/abs/2403.06764>.
- [3] Lin Chen, Jisong Li, Xiaoyi Dong, Pan Zhang, Conghui He, Jiaqi Wang, Feng Zhao, and Dahua Lin. Sharegpt4v: Improving large multi-modal models with better captions. *arXiv preprint arXiv:2311.12793*, 2023.
- [4] Zhe Chen, Weiyun Wang, Yue Cao, Yangzhou Liu, Zhangwei Gao, Erfei Cui, Jinguo Zhu, Shenglong Ye, Hao Tian, Zhaoyang Liu, et al. Expanding performance boundaries of open-source multimodal models with model, data, and test-time scaling. *arXiv preprint arXiv:2412.05271*, 2024.
- [5] Zhe Chen, Weiyun Wang, Hao Tian, Shenglong Ye, Zhangwei Gao, Erfei Cui, Wenwen Tong, Kongzhi Hu, Jiapeng Luo, Zheng Ma, et al. How far are we to gpt-4v? closing the gap to commercial multimodal models with open-source suites. *Science China Information Sciences*, 67(12):220101, 2024.
- [6] Zhe Chen, Jiannan Wu, Wenhai Wang, Weijie Su, Guo Chen, Sen Xing, Muyan Zhong, Qinglong Zhang, Xizhou Zhu, Lewei Lu, et al. Internvl: Scaling up vision foundation models and aligning for generic visual-linguistic tasks. In *Proceedings of the IEEE/CVF Conference on Computer Vision and Pattern Recognition*, pages 24185–24198, 2024.
- [7] Maha Elbayad, Jiatao Gu, Edouard Grave, and Michael Auli. Depth-adaptive transformer. *arXiv preprint arXiv:1910.10073*, 2019.
- [8] Peng Gao, Shijie Geng, Renrui Zhang, Teli Ma, Rongyao Fang, Yongfeng Zhang, Hongsheng Li, and Yu Qiao. Clip-adapter: Better vision-language models with feature adapters. *International Journal of Computer Vision*, 132(2):581–595, 2024.
- [9] Zhangwei Gao, Zhe Chen, Erfei Cui, Yiming Ren, Weiyun Wang, Jinguo Zhu, Hao Tian, Shenglong Ye, Junjun He, Xizhou Zhu, et al. Mini-internvl: a flexible-transfer pocket multi-modal model with 5% parameters and 90% performance. *Visual Intelligence*, 2(1):1–17, 2024.
- [10] Agrim Gupta, Piotr Dollar, and Ross Girshick. LVIS: A dataset for large vocabulary instance segmentation. In *Proceedings of the IEEE/CVF conference on computer vision and pattern recognition*, pages 5356–5364, 2019.
- [11] Can Jin, Tianjin Huang, Yihua Zhang, Mykola Pechenizkiy, Sijia Liu, Shiwei Liu, and Tianlong Chen. Visual prompting upgrades neural network sparsification: A data-model perspective. In *Proceedings of the AAAI Conference on Artificial Intelligence*, volume 39, pages 4111–4119, 2025.
- [12] Can Jin, Ying Li, Mingyu Zhao, Shiyu Zhao, Zhenting Wang, Xiaoxiao He, Ligong Han, Tong Che, and Dimitris N. Metaxas. Lor-VP: Low-rank visual prompting for efficient vision model adaptation. In *The Thirteenth International Conference on Learning Representations*, 2025. URL <https://openreview.net/forum?id=5btFIv2PNb>.
- [13] Aniruddha Kembhavi, Mike Salvato, Eric Kolve, Minjoon Seo, Hannaneh Hajishirzi, and Ali Farhadi. A diagram is worth a dozen images. In *Computer Vision—ECCV 2016: 14th European Conference, Amsterdam, The Netherlands, October 11–14, 2016, Proceedings, Part IV 14*, pages 235–251. Springer, 2016.
- [14] Junnan Li, Dongxu Li, Caiming Xiong, and Steven Hoi. Blip: Bootstrapping language-image pre-training for unified vision-language understanding and generation. In *International conference on machine learning*, pages 12888–12900. PMLR, 2022.

- [15] Junnan Li, Dongxu Li, Silvio Savarese, and Steven Hoi. Blip-2: Bootstrapping language-image pre-training with frozen image encoders and large language models. In *International conference on machine learning*, pages 19730–19742. PMLR, 2023.
- [16] Liunian Li, Zi-Yi Dou, Nanyun Peng, and Kai-Wei Chang. Desco: Learning object recognition with rich language descriptions. *Advances in Neural Information Processing Systems*, 36: 37511–37526, 2023.
- [17] Liunian Harold Li, Pengchuan Zhang, Haotian Zhang, Jianwei Yang, Chunyuan Li, Yiwu Zhong, Lijuan Wang, Lu Yuan, Lei Zhang, Jenq-Neng Hwang, et al. Grounded language-image pre-training. In *Proceedings of the IEEE/CVF Conference on Computer Vision and Pattern Recognition*, pages 10965–10975, 2022.
- [18] Chuang Lin, Yi Jiang, Lizhen Qu, Zehuan Yuan, and Jianfei Cai. Generative region-language pretraining for open-ended object detection. In *Proceedings of the IEEE/CVF Conference on Computer Vision and Pattern Recognition*, pages 13958–13968, 2024.
- [19] Haotian Liu, Chunyuan Li, Qingyang Wu, and Yong Jae Lee. Visual instruction tuning. *Advances in neural information processing systems*, 36:34892–34916, 2023.
- [20] Haotian Liu, Chunyuan Li, Qingyang Wu, and Yong Jae Lee. Visual instruction tuning. *Advances in neural information processing systems*, 36, 2024.
- [21] Shilong Liu, Zhaoyang Zeng, Tianhe Ren, Feng Li, Hao Zhang, Jie Yang, Qing Jiang, Chunyuan Li, Jianwei Yang, Hang Su, et al. Grounding dino: Marrying dino with grounded pre-training for open-set object detection. In *European Conference on Computer Vision*, pages 38–55. Springer, 2024.
- [22] Ze Liu, Yutong Lin, Yue Cao, Han Hu, Yixuan Wei, Zheng Zhang, Stephen Lin, and Baining Guo. Swin transformer: Hierarchical vision transformer using shifted windows. In *Proceedings of the IEEE/CVF International Conference on Computer Vision (ICCV)*, 2021.
- [23] Yanxin Long, Jianhua Han, Runhui Huang, Hang Xu, Yi Zhu, Chunjing Xu, and Xiaodan Liang. Fine-grained visual-text prompt-driven self-training for open-vocabulary object detection. *IEEE Transactions on Neural Networks and Learning Systems*, 2023.
- [24] Ahmed Masry, Do Long, Jia Qing Tan, Shafiq Joty, and Enamul Hoque. ChartQA: A benchmark for question answering about charts with visual and logical reasoning. In *Findings of the Association for Computational Linguistics: ACL 2022*, pages 2263–2279, Dublin, Ireland, May 2022. Association for Computational Linguistics. doi: 10.18653/v1/2022.findings-acl.177. URL <https://aclanthology.org/2022.findings-acl.177>.
- [25] Minesh Mathew, Dimosthenis Karatzas, and CV Jawahar. Docvqa: A dataset for vqa on document images. In *Proceedings of the IEEE/CVF winter conference on applications of computer vision*, pages 2200–2209, 2021.
- [26] Matthias Minderer, Alexey Gritsenko, and Neil Houlsby. Scaling open-vocabulary object detection. *Advances in Neural Information Processing Systems*, 36:72983–73007, 2023.
- [27] Alec Radford, Jong Wook Kim, Chris Hallacy, Aditya Ramesh, Gabriel Goh, Sandhini Agarwal, Girish Sastry, Amanda Askell, Pamela Mishkin, Jack Clark, et al. Learning transferable visual models from natural language supervision. In *International conference on machine learning*, pages 8748–8763. PMLR, 2021.
- [28] Tianhe Ren, Yihao Chen, Qing Jiang, Zhaoyang Zeng, Yuda Xiong, Wenlong Liu, Zhengyu Ma, Junyi Shen, Yuan Gao, Xiaoke Jiang, et al. Dino-x: A unified vision model for open-world object detection and understanding. *arXiv preprint arXiv:2411.14347*, 2024.
- [29] Anna Rohrbach, Lisa Anne Hendricks, Kaylee Burns, Trevor Darrell, and Kate Saenko. Object hallucination in image captioning. *arXiv preprint arXiv:1809.02156*, 2018.
- [30] Samuel Schuster, Yumin Suh, Konstantinos M Dafnis, Zhixing Zhang, Shiyu Zhao, Dimitris Metaxas, et al. Omnilabel: A challenging benchmark for language-based object detection. In *Proceedings of the IEEE/CVF International Conference on Computer Vision*, pages 11953–11962, 2023.

- [31] Shuai Shao, Zeming Li, Tianyuan Zhang, Chao Peng, Gang Yu, Xiangyu Zhang, Jing Li, and Jian Sun. Objects365: A large-scale, high-quality dataset for object detection. In *Proceedings of the IEEE/CVF international conference on computer vision*, pages 8430–8439, 2019.
- [32] Weiyun Wang, Zhe Chen, Wenhai Wang, Yue Cao, Yangzhou Liu, Zhangwei Gao, Jinguo Zhu, Xizhou Zhu, Lewei Lu, Yu Qiao, and Jifeng Dai. Enhancing the reasoning ability of multimodal large language models via mixed preference optimization. *arXiv preprint arXiv:2411.10442*, 2024.
- [33] Chi Xie, Zhao Zhang, Yixuan Wu, Feng Zhu, Rui Zhao, and Shuang Liang. Described object detection: Liberating object detection with flexible expressions. *Advances in Neural Information Processing Systems*, 36:79095–79107, 2023.
- [34] An Yang, Baosong Yang, Binyuan Hui, Bo Zheng, Bowen Yu, Chang Zhou, Chengpeng Li, C Li, D Liu, F Huang, et al. Qwen2 technical report. *arXiv preprint arXiv:2407.10671*, 2024.
- [35] Lewei Yao, Jianhua Han, Youpeng Wen, Xiaodan Liang, Dan Xu, Wei Zhang, Zhenguo Li, Chunjing Xu, and Hang Xu. Detclip: Dictionary-enriched visual-concept paralleled pre-training for open-world detection. *Advances in Neural Information Processing Systems*, 35:9125–9138, 2022.
- [36] Lewei Yao, Renjie Pi, Jianhua Han, Xiaodan Liang, Hang Xu, Wei Zhang, Zhenguo Li, and Dan Xu. Detclipv3: Towards versatile generative open-vocabulary object detection. In *Proceedings of the IEEE/CVF Conference on Computer Vision and Pattern Recognition*, pages 27391–27401, 2024.
- [37] Shukang Yin, Chaoyou Fu, Sirui Zhao, Tong Xu, Hao Wang, Dianbo Sui, Yunhang Shen, Ke Li, Xing Sun, and Enhong Chen. Woodpecker: Hallucination correction for multimodal large language models. *Science China Information Sciences*, 67(12):220105, 2024.
- [38] Haoxuan You, Haotian Zhang, Zhe Gan, Xianzhi Du, Bowen Zhang, Zirui Wang, Liangliang Cao, Shih-Fu Chang, and Yinfei Yang. Ferret: Refer and ground anything anywhere at any granularity. *arXiv preprint arXiv:2310.07704*, 2023.
- [39] Peter Young, Alice Lai, Micah Hodosh, and Julia Hockenmaier. From image descriptions to visual denotations: New similarity metrics for semantic inference over event descriptions. *Transactions of the association for computational linguistics*, 2:67–78, 2014.
- [40] Licheng Yu, Patrick Poirson, Shan Yang, Alexander C Berg, and Tamara L Berg. Modeling context in referring expressions. In *Computer Vision—ECCV 2016: 14th European Conference, Amsterdam, The Netherlands, October 11–14, 2016, Proceedings, Part II 14*, pages 69–85. Springer, 2016.
- [41] Alireza Zareian, Kevin Dela Rosa, Derek Hao Hu, and Shih-Fu Chang. Open-vocabulary object detection using captions. In *Proceedings of the IEEE/CVF Conference on Computer Vision and Pattern Recognition*, pages 14393–14402, 2021.
- [42] Bohan Zhai, Shijia Yang, Chenfeng Xu, Sheng Shen, Kurt Keutzer, Chunyuan Li, and Manling Li. Halle-control: controlling object hallucination in large multimodal models. *arXiv preprint arXiv:2310.01779*, 2023.
- [43] Hao Zhang, Feng Li, Shilong Liu, Lei Zhang, Hang Su, Jun Zhu, Lionel M Ni, and Heung-Yeung Shum. Dino: Detr with improved denoising anchor boxes for end-to-end object detection. *arXiv preprint arXiv:2203.03605*, 2022.
- [44] Renrui Zhang, Jiaming Han, Chris Liu, Peng Gao, Aojun Zhou, Xiangfei Hu, Shilin Yan, Pan Lu, Hongsheng Li, and Yu Qiao. Llama-adapter: Efficient fine-tuning of language models with zero-init attention. *arXiv preprint arXiv:2303.16199*, 2023.
- [45] Shiyu Zhao, Zhixing Zhang, Samuel Schuster, Long Zhao, BG Vijay Kumar, Anastasis Sathopoulos, Manmohan Chandraker, and Dimitris N Metaxas. Exploiting unlabeled data with vision and language models for object detection. In *European conference on computer vision*, pages 159–175. Springer, 2022.

- [46] Shiyu Zhao, Samuel Schuster, Long Zhao, Zhixing Zhang, Yumin Suh, Manmohan Chandraker, Dimitris N Metaxas, et al. Taming self-training for open-vocabulary object detection. In *Proceedings of the IEEE/CVF Conference on Computer Vision and Pattern Recognition*, pages 13938–13947, 2024.
- [47] Shiyu Zhao, Long Zhao, Yumin Suh, Dimitris N Metaxas, Manmohan Chandraker, Samuel Schuster, et al. Generating enhanced negatives for training language-based object detectors. In *Proceedings of the IEEE/CVF Conference on Computer Vision and Pattern Recognition*, pages 13592–13602, 2024.
- [48] Wei Li Zuwei Long. Open grounding dino:the third party implementation of the paper grounding dino. <https://github.com/longzw1997/Open-GroundingDino>, 2023.

A Experiment Details

A.1 Attention Maps in Qwen2-0.5B Decoding

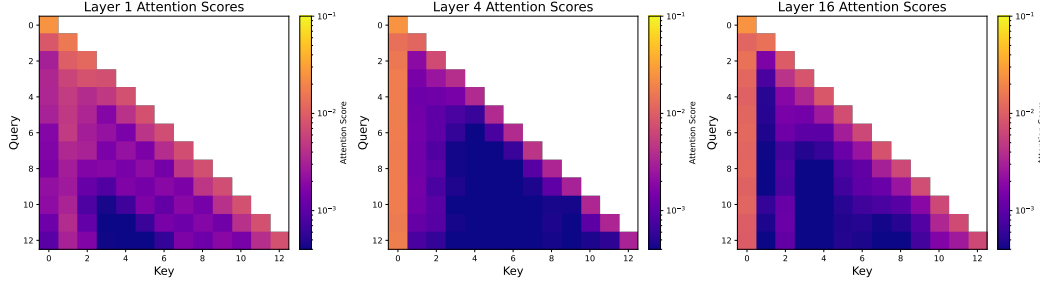


Figure 6: Attention maps during the decoding process of Qwen2-0.5B.

Based on the attention maps during the decoding process of Qwen2-0.5B, We draw the attention scores for different layer as follow:

$$\text{Attention Score}(Q, K) = \frac{QK^T}{\sqrt{d_k}} \quad (10)$$

Where, Q, K are the Query and Key matrix in the transformer Decoder layer, $\text{softmax}(\cdot)$ as show in Figure 6, we have reached an approximate conclusion [2]. We can observe that in the first layer, attention is distributed relatively smoothly across different types of tokens. In the deeper layers, starting from local attention, attention scores are aggregated onto system prompts, instructions, and output tokens, while attention to image tokens becomes quite sparse. In the deeper layers, there are strong vertical lines (in the system prompts) that dominate most of the attention scores. The presence of these strong vertical lines indicates that certain input tokens remain highly attended to throughout the decoding process. If large-scale, high-intensity attention to image tokens were also maintained in the deeper layers, it would suggest that a significant amount of visual information is still needed for inference at those stages. However, as seen in the visualization, the deeper layers primarily focus on some key text tokens, which precisely indicates that the processing of images has already been completed in the earlier layers, and most of the image information has been "condensed" into the representations.

A.2 Adapter Architecture Detail

Architecture I (Double Cross-Modal Fusion).

As show in Figure 7, this design leverages two sequential cross-attention layers to incorporate both textual and visual cues into the Detector. First, the image embeddings E_{VL} attend to text embeddings E_T , ensuring high-level semantic alignment via a *text-guided image fusion*. Second, the fused features further guide the Detector through a *prompt-enhanced detection* stage, where Detector queries attend to the fused representation. A zero-initialized gating mechanism adaptively combines these cross-modal features back into the Detector's backbone.

Architecture II, III (Late Prompt Projection).

As show in Figure 8, we remove the second cross-attention step to streamline the flow into the Detector. A 3×3 convolution directly transforms the fused adaptation prompts into the compatible feature dimension before feeding them into the final cross-modal decoder.

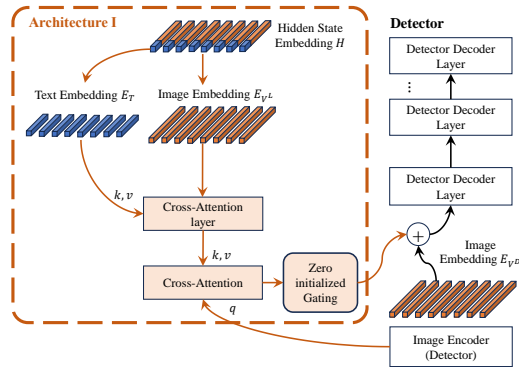


Figure 7: The adapter architecture I of our approach.

A.3 Experiment Configuration

All experiments are conducted on eight NVIDIA A100 GPUs. During Stage 1 (pre-training) and Stage 2 (fine-tuning), we train the MLP layer for exactly one epoch each. For pre-training we use a batch size of 128, a learning rate of 1×10^{-3} , weight decay of 0.03, and no warm-up. For fine-tuning, the warm-up ratio is set to 0.03, while the batch size, learning rate, and weight decay are fixed at 128, 4×10^{-5} , and 0, respectively. In Stage 3 we train the adapter for one epoch with a batch size of 64, employing cosine learning-rate scheduling (base learning rate 2×10^{-4}) without warm-up or weight decay. The MLP layer and the LLM are co-trained with the adapter using a separate learning rate of 4×10^{-5} .

The hyper-parameters for Stages 1–3 are summarised in Table 7a. To investigate the impact of model scale, we vary LLM parameter sizes as detailed in Table 7b, with the results reported in Section 4.2.3. Table 7c lists the settings used to evaluate alternative adapter architectures; the corresponding OmniLabel scores appear in Table 3. Finally, Table 7d specifies the setup for examining different decoder layers, and the ablation results are presented in Section 4.4.

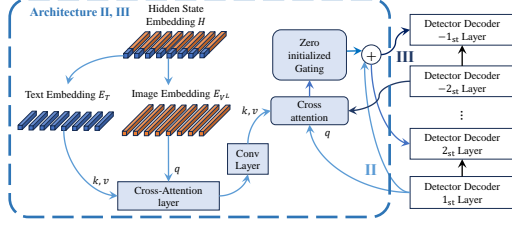


Figure 8: The adapter architecture II, III of our approach.

(a) Vision Decoder Share from Detector		(b) Different MLLMs	
MLLM	InternVL2-1B	MLLM	InternVL2: 1B, 2B, 8B
ℓ_{LM}	2	ℓ_{LM}	2
AP to ℓ_D	6	AP to ℓ_D	6
Train Dataset	Object365, COCO, Flickr30k	Train Dataset	Object365, COCO, Flickr30k
Stage 1 lr	MLP: $1e^{-3}$	adapter arch.	IV
Stage 2 lr	MLP: $2e^{-5}$		
Stage 3 lr	MLP & Adapter: $2e^{-4}$, LLM: $2e^{-5}$		
Adapter arch.	IV		

(a) Experiment configuration details for vision decoder share from detector.

(b) Experiment configuration details for different LLMs.

(c) Adapter Architectures		(d) Ablations: Decoder Layers	
MLLM	InternVL2-2B	MLLM	InternVL2-1B
ℓ_{LM}	8	ℓ_{LM}	-1, 2, 4, 8, 24
AP to ℓ_D	1, 6	AP to ℓ_D	6
Train Dataset	COCO, Flickr30k	Train Dataset	Object365, COCO, Flickr30k
		adapter arch.	IV

(c) Experiment configuration details for different adapter architectures.

(d) Ablation details for different decoder layers.

Table 7: Experiment configuration summary.

A.4 Dynamic Image Processing

In Section 4.2.3 and Section 4.4, Since the MLLM and Detector’s Image encoder process the same image in a single inference, and considering that the Hidden state cropped from the Vision token positions in LLMs corresponds to the Vision Embedding processed by the detector, we are inspired by LLaVA[19]’s approach to dynamic image processing. The Vision Embedding sent to LLMs is processed as shown in Figure 9. For a given image, based on a 448×448 patch, rectangles are generated from a 1:3 to 3:1 aspect ratio and matched to the image. The image is then padded to the smallest rectangle that can contain the original image and sent to the Vision Transformer (ViT) of LLMs. The size of the patch embedding should be $448/(14 \times \text{scale factor} = 2) = 16$. Finally, the ViT embedding is cropped according to the previous padding ratio to restore the original image’s aspect ratio.

MME	InternVL2-1B	Swin-T & Qwen2-0.5B
total	1363	1027
existence	180.0	158.3
count	118.3	105.0
position	126.7	66.7
color	135.0	128.3
posters	110.2	75.9
celebrity	146.8	131.8
scene	148.5	120.8
landmark	132.5	83.3
artwork	140.0	80.0
OCR	125.0	77.5
total	419.29	273.57
commonsense reasoning	99.29	68.57
numerical calculation	62.50	62.50
text translation	162.50	70.00
code reasoning	95.00	72.50

Table 8: Performance comparison of InternVL2-1B, Swin-T & Qwen2-0.5B on MME Perception and Cognition tasks.

A.5 MLLM Alignment (Swin-T & Qwen2-0.5B)

We evaluated the alignment of Swin-T & Qwen2-0.5B on MME and compared it with the original method of InternVL2-1B (InternVL Vit & Qwen2-0.5B) as show in Table 8. To evaluate the impact of replacing the vision encoder and aligning the LLM on MLLM performance, we compared the score gaps between InternVL2-1B and Swin-T & Qwen2-0.5B on the MME benchmark. Compared to InternVL2-1B, Swin-T & Qwen2-0.5B scored 1027 on perception, a decrease of 335 (InternVL2-1B scored 1362.97), and 273.57 on cognition, a decrease of 145.72 (InternVL2-1B scored 419.29). It is worth noting that, although more advanced alignment strategies may exist, our work does not aim to achieve maximum alignment between an extremely lightweight vision encoder (Swin-Tiny) and the LLM, particularly without employing strategies such as Dynamic Tiling.

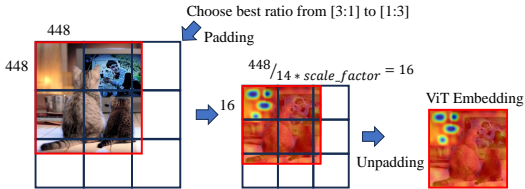


Figure 9: Dynamic Image Processing

B Why MLLM Hidden States Cannot Replace Visual Detectors

One might be tempted to ask: “Can we simply replace a specialized visual detector with a LLM, MLLM or VLM and still achieve comparable performance?” To answer this question, Table 9 presents a head-to-head comparison between our detector-based pipeline and an end-to-end LLM approach across multiple benchmarks. As the results make clear, relying solely on the LLM without a dedicated object detector leads to a substantial drop in accuracy and consistency.

GROUNDINGDINO-PRE establishes a detector base on Open-GroundingDINO [21] that has *never* been exposed to COCO, being trained only on Objects365, GoldG, and Cap4M; GROUNDINGDINO-COCO SFT fine-tunes the same weights on COCO SWINTINY-BERT serves as a *vision-only* control whose Swin-Tiny backbone and BERT text branch use only same framework as Open-GroundingDINO [21] is identical to that used in the multi-modal runs yet, like the MLLMs, has never seen COCO or any object-detection data. The three substitution variants—LLaVA-L8, IVL2-L2, and IVL2-L8—replace the Swin feature map with hidden states taken from decoder layers 2 or 8 of LLaVA-1.5 or InternVL-2B, enabling a direct test of whether raw MLLM representations can stand in for detector-oriented visual embeddings.

As show int the Table 9, fine-tuning the vision backbone on COCO (GDINO-COCO) improves $AP_{50:95}$ by **+26** points over its out-of-domain counterpart, underscoring the importance of spatial

Table 9: **Detector vs. MLLM Hidden-State Features on COCO-2017 val.** Baselines are two GroundingDINO variants and vision-only SwinTiny-BERT; substitutions plug frozen decoder states from LLaVA-1.5 (L8) or InternVL-2B (L2/L8).

Method	AP _{50:95}	AP ₅₀	AP ₇₅
GROUNDINGDINO-PRE	31.23	44.37	34.09
GROUNDINGDINO-COCO SFT	57.23	73.27	63.18
SWINTINY-BERT	41.97	57.45	45.85
LLAVA-L8	24.19	39.47	24.94
IVL2-L2	38.28	55.25	41.18
IVL2-L8	42.64	63.77	44.92

alignment learned from explicit detection supervision. By contrast, treating language-vision model (MLLM) activations as a drop-in surrogate for visual tokens is ineffective: the strongest variant (IVL2-L8) still trails the fully visual SWINTINY-BERT by -0.67 AP_{50:95} and remains -14.6 points below the COCO-tuned baseline. The gap widens to -33 points when substituting LLAVA-L8, revealing that decoder-layer semantics alone carry minimal localisation cues.

This discrepancy arises because MLLM hidden states are produced after heavy token mixing and rotary positional encoding optimised for caption generation; they lack the multi-scale geometry and inductive biases embedded in convolutional or ViT backbones. Without an explicit fusion mechanism that jointly conditions on language and vision, the detector cannot recover accurate object coordinates, leading to systematic localisation failure. The comparison between SWINTINY-BERT (whose Swin weights, like the MLLMs, have *never* seen COCO) and the substitution runs highlights the central claim of this study: **knowledge fusion is indispensable—naive replacement of visual embeddings with isolated MLLM features is not a viable route to open-vocabulary detection.**

C Case Study

We compared test results on OmniLabel using InternVL2-1B for adaptation prompts against directly applying GroundingDINO on selected samples. We excluded all category-based targets and focused solely on the detection performance of descriptive targets. As shown in Figure 10, GroundingDINO struggles to understand target descriptions involving quantities, states, ages, colors, or spatial relationships. However, when the LLM provides semantic-level understanding, the detector’s ability to recognize such targets improves significantly.

Notably, the adaptation prompt functions as expected, guiding the detector rather than allowing the adapter to dominate the grounding task. As seen in the recognition results in Figure 10, GroundingDINO often fails to locate individuals, instead detecting entire objects, as in the case of "The computer monitors on the desk that are turned on." Additionally, it struggles to interpret positional relationships in text descriptions, such as "the sandwiches that are each on the same plate with the other." With the adaptation prompt, the detector retains an overall understanding while incorporating individual positional relationships. Furthermore, it corrects errors in spatial logic relationships.

D Implementation Details

D.1 Dataset Introduction

Table 10 provides the attributes, sizes, and functional descriptions of all datasets used in our stages 1, 2, 3 and evaluation, to illustrate the support they offer during the process. All datasets are distributed under licences that permit non-commercial academic research.

D.2 Model Introduction

To foster clarity and reproducibility, we first outline the *functional role* of every third-party model or code base incorporated into LED (Table 11).

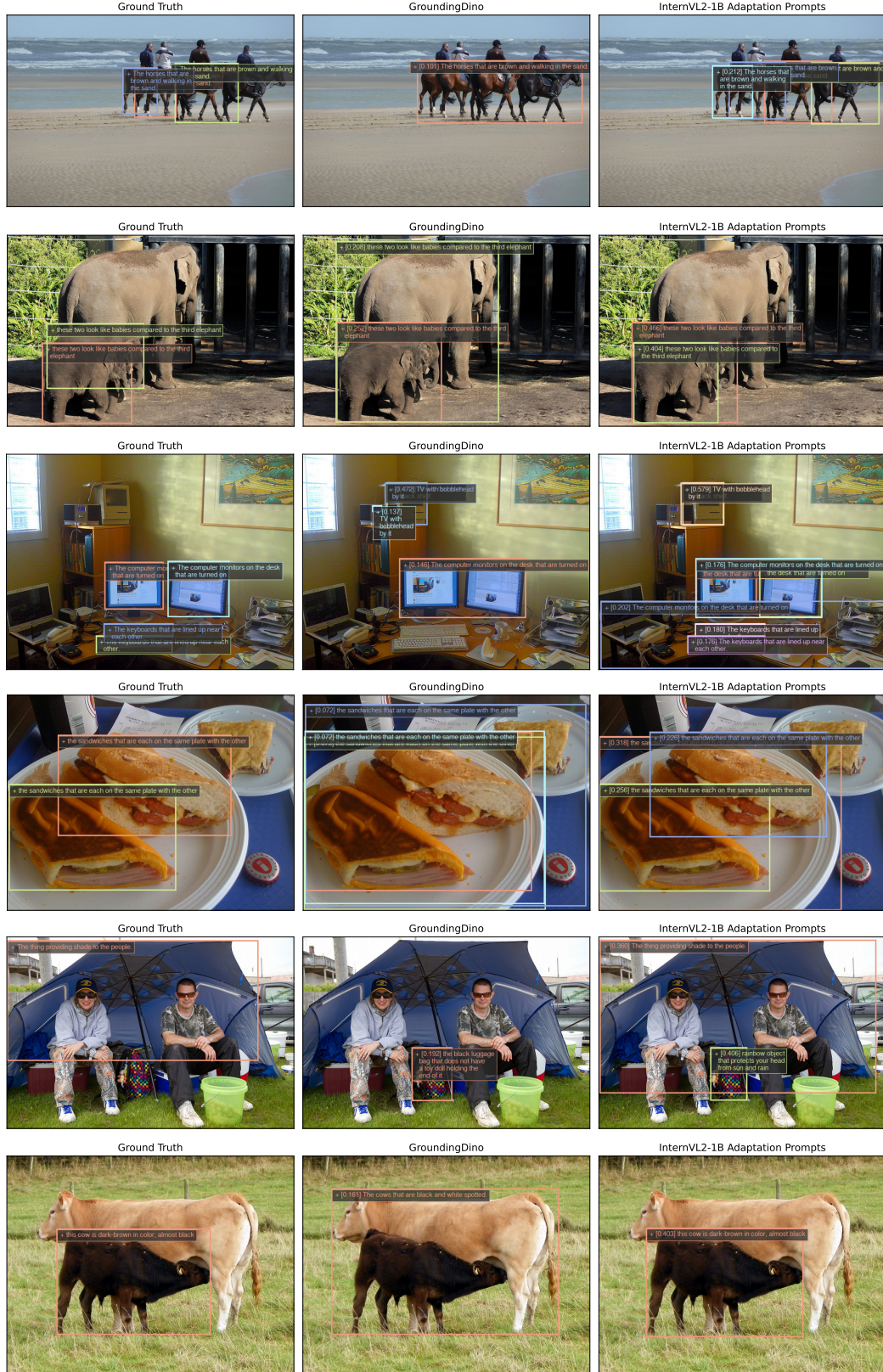


Figure 10: Case Study for OmniLabel using InternVL2-1B to provide adaptation prompts versus directly using GroundingDINO.

Table 10: Introduction of datasets used in stage 1, stage 2, and stage 3.

Dataset	Introduction
<i>Pretraining Data for Stage 1</i>	
LAION-CC-SBU 558K	The LAION-CC-SBU dataset is a curated subset of the LAION, Conceptual Captions (CC), and SBU datasets. It comprises 558K image-caption pairs for the pretraining stage for feature alignment in visual instruction tuning. [19]
<i>Instruction Tuning Data for Stage 2</i>	
ShareGPT4V	ShareGPT4V dataset is curated from LAION, CC, SBU, SAM, COCO, web-landmark, web-celebrity, wikiart, etc, resulting in total 102K high-quality image-text pairs with the help of powerful GPT4-Vision [3].
SFT	SFT dataset comprises approximately 665K multimodal instruction-following samples, facilitating improved alignment of visual-language models to human instructions [3].
ChartQA	ChartQA is a domain-specific visual question-answering dataset containing 18K samples designed explicitly for interpreting various types of charts, including bar graphs, pie charts, and line plots. [24]
AI2D	AI2D includes approximately 12K annotated diagrams paired with structured question-answer data, particularly aimed at evaluating multimodal reasoning over scientific diagrams. [13]
DocVQA	DocVQA contains 10K samples that involve complex question-answering tasks over visually rich document images, emphasizing text recognition, layout analysis, and semantic comprehension. [25]
<i>Grounding Data for Stage 3</i>	
Objects365	Objects365 is a large-scale object detection dataset featuring over 1.7 million images with dense annotations covering 365 common object categories, enhancing general object detection capabilities. [31]
COCO2017	COCO2017 provides around 118K training images annotated for object detection, and captioning tasks, widely used as a benchmark in computer vision research.
Flickr30k	Flickr30k is a standard multimodal dataset with 31K images, each annotated with five descriptive captions, commonly utilized for improving image captioning and cross-modal retrieval tasks. [39]
<i>Evaluation Data</i>	
RefCOCO+/+g	The RefCOCO+/+g datasets consist of referring expression comprehension tasks, where models must identify objects in images based on natural language descriptions. REFCOCO has approximately 142K referring expressions, while RefFCOCO+ and RefCOCOg provide more challenging and generalized scenarios. [40]
Omnilabel	Omnilabel is a multimodal benchmark dataset containing diverse visual-language tasks designed to comprehensively evaluate the generalization and zero-shot capabilities of visual-language models across various tasks and domains. [30]

E Broader Impacts

Potential benefits. By enabling *lightweight open-vocabulary grounding* with minor extra FLOPs, LED can (i) improve on-device perception for assistive robotics and smart prosthetics; (ii) lower the computational barrier for researchers in low-resource regions to experiment with vision-language models; and (iii) accelerate scientific discovery in ecology, astronomy, and digital humanities, where long-tail object categories are common.

Potential harms. Hallucinating an object that is not present—could propagate misinformation through downstream captioning or retrieval systems. Biases inherited from pre-training corpora

Table 11: Concise introductions for third-party models and code bases.

Model / Code	Introduction
Qwen2-0.5B	A 0.5-billion-parameter decoder-only LLM trained on ~ 2 T multi-lingual tokens; we tap its early hidden states for knowledge fusion in Stage 3 of LED [34].
InternVL2 (1 B / 2 B / 8 B)	A family of vision–language foundation models pretrained on 20 M image–text pairs; the 1 B and 2 B variants are used as alternative language decoders in our ablations [16, 26, 36, 45, 46].
LLaVA-1.5	An open-source multimodal chat model aligning a CLIP vision encoder with a Vicuna language head via instruction tuning; included as an external baseline for grounding performance [20].
Open-GroundingDINO	An open-vocabulary detector that couples a Swin-Tiny backbone with a text encoder; serves as the base detector into which our LED adapters are inserted [21].
Swin-Tiny	A hierarchical vision encoder pretrained on ImageNet-22K; provides four-stage feature maps consumed by the detector backbone [22].

may yield disparate false-positive rates across demographic groups, disproportionately affecting already-marginalised communities.

Mitigation strategies. More advanced models and algorithms. As the LLM field continues to advance, the Hallucinating problem will continue to be overcome and optimized. **Research-only weight release.** Pre-trained weights will initially be released under an academic non-commercial licence; commercial use will require a separate agreement that enforces compliance with a no-surveillance clause. **Transparent data lineage.** All training datasets are listed with licences and provenance (Section D.1); no proprietary or private images were used, reducing privacy concerns at source.